High Quality Factor Mode Ordered Dual Foucault Pendulum Gyroscope

Mohammad H. Asadian*, Sina Askari*, Ian B. Flader†, Yunhan Chen†, Dustin D. Gerrard†, Dongsuk D. Shin†, Hyun-Keun Kwon†, Thomas W. Kenny†, and Andrei M. Shkel*
*Microsystems Lab, University of California, Irvine, CA, USA
†Micro Structures and Sensors Lab, Stanford University, Palo Alto, CA, USA

***Abstract*—This paper presents the implementation of a coupling mechanism on dynamically-balanced Dual Foucault Pendulum (DFP) gyroscopes, ordering the anti-phase and in-phase modes of vibration. A wide frequency separation is achieved between the desired anti-phase and the spurious in-phase resonance. Mode ordering of dual mass tuning fork gyroscopes provides isolation of the anti-phase resonance, resulting in the reduction of energy losses through mode conversion and improves common-mode rejection. A mode ordered Dual Foucault Pendulum (DFP) gyroscope at an operational frequency of 15 kHz was fabricated using the wafer-level epitaxial silicon encapsulation process. The quality factor higher than 700,000 was achieved after vacuum sealing with an activated getter. The coupling mechanism was explained and initial rate characterization of the device was reported.**

I. Introduction

Microelectromechanical Systems (MEMS) gyroscopes with high quality factor and rejection of linear acceleration and vibration can be utilized for reliable and accurate angular rate measurement for navigation applications. The quality factor is the metric that indicates the dissipation of energy in a resonant structure. The main energy dissipation mechanisms in MEMS resonators and gyroscopes are (1) air damping, (2) anchor losses, (3) thermoelastic damping (TED), and (4) mode conversion losses [1]. The air damping is the major source of energy dissipation, unless the vibratory device is operated in a high-vacuum encapsulation. The anchor loss, TED, and mode conversion loss depend on the structural design, mode of operation, and fabrication imperfections. In an ideal case, a dynamically-balanced structure mitigates the dissipation of energy through the substrate, as the net reaction forces and moments acting on the anchors are minimized [2]. Moreover, a large separation between the operational mode and spurious modes minimizes the mode conversion losses from mode coupling due to fabrication imperfections [3]. The TED and mode conversion losses can be mitigated by the geometric and structural design of suspension elements and arrangement of coupling mechanisms.

In the tuning fork microresonators and gyroscopes, two (or more) proof masses are mechanically coupled by flexural springs and driven in anti-phase motion [4]. The tuning fork MEMS gyroscopes operated in a degenerate mode (mode-matched), demonstrated high sensitivity to the input rotation and low-noise performance [5]–[8]. However, the additional degrees of freedom in devices with multiple lumped masses introduce spurious frequency modes in addition to the operational mode. These spurious modes can cause leakage of the vibrational energy or be excited by common-mode linear acceleration and vibration.

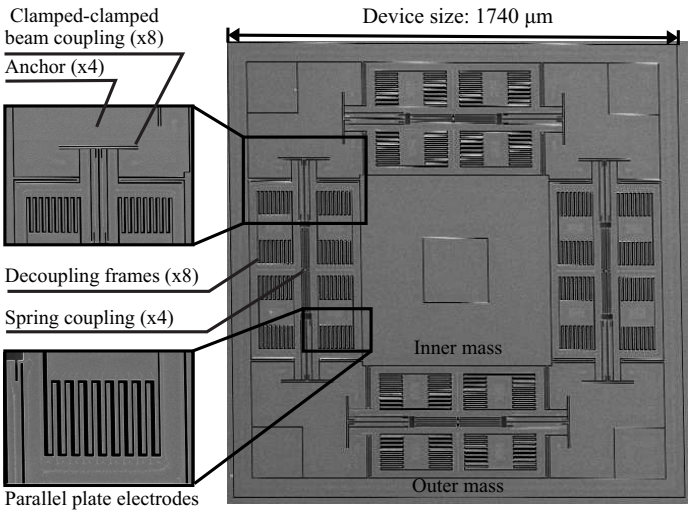

Fig. 1. Mode-ordered DFP with fully differential parallel plate drive and sense electrodes fabricated using silicon epitaxial encapsulation process. The device footprint is $< 1.8 \times 1.8\ mm^2$.

In this work, a coupling mechanism is implemented on a Dual Foucault Pendulum (DFP) [5] structure that provides large frequency separation between anti-phase and spurious in-phase modes with the anti-phase mode ordered as the lowest frequency mode.

II. Mode Ordered Dual Foucault Pendulum

The mode ordered DFP MEMS gyroscope was fabricated on a Silicon-on-Insulator (SOI) wafer with $40\ \mu m$ device thickness in a wafer-level epitaxial silicon encapsulation process with fully differential parallel-plate electrodes [9]. The X-Y symmetric design of the device consists of two identical proof masses, mechanically coupled using four folded beam springs and anchored through four pairs of internal beam elements. The beam elements clamped at both ends to the anchors, isolating the proof mass motion from the substrate, Fig. 1. The parallel plate electrodes were designed with 1.5 μm capacitive gas and 4.5 μm anti-gap, forming an active capacitance of 1.5 pF at each drive and pickoff channel. The parallel-plate electrodes provide fully differential excitation and detection as well as electrostatic frequency tuning. Four pairs of decoupling

978-1-5386-4707-3/18/$31.00 ©2018 IEEE

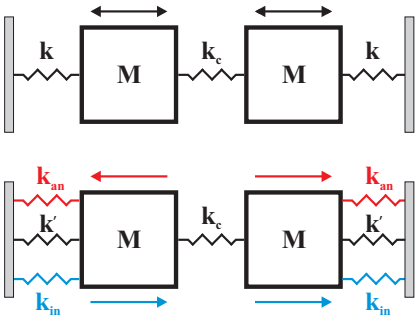

Fig. 2. (top) Schematic of mass-spring coupling in dual mass gyroscope with a weak spring coupling (k_c), (bottom) a clamped-clamped beam provides different coupling stiffnesses for in-phase and anti-phase modes ($k_{in} > k_{an}$), both cases represent one axis of a dual mass tuning fork gyroscope.

frames were implemented to restrict the motion of electrodes in one direction and reduce the cross-coupling between the X-axis and the Y-axis.

Fig. 2 schematically demonstrates the coupling mechanisms in a regular and a mode-ordered configuration with the clamped-clamped beam element designs. The resonance frequency of the in-phase, ω_{in}, and anti-phase, ω_{in}, in a regular dual mass resonator with two identical proof masses, M, and two identical spring elements, k, and a coupling spring, k_c, are:

$$\omega_{in} = \sqrt{\frac{k}{M}},\ \omega_{an} = \sqrt{\frac{k + 2k_c}{M}} \tag{1}$$

The coupling stiffness acts upon the anti-phase mode of vibration, resulting in a higher resonance frequency in anti-phase motion compared to the in-phase motion. The low-frequency in-phase mode makes the gyroscope susceptible to the linear acceleration. Moreover, weak coupling stiffness, $k_c << k$, would bring the resonant frequency of the two modes in close proximity and result in the mode conversion losses.

The concept of using an internal clamped-clamped beam element was implemented in a Quad Mass Gyroscope (QMG) as a negative coupling stiffness between the proof masses in the anti-phase mode [10]. Here, a similar concept was implemented by anchoring the proof masses through a clamped-clamped beam element to impose a different in-phase, k_{in}, and anti-phase stiffnesses, k_{an}. Thus, ordering the anti-phase and in-phase modes of the device. The internal beam resonates at its 1^{st} flexural bending mode when proof masses move in opposite directions and at its 2^{nd} flexural bending mode when the proof masses move in the same direction, Fig. 3. In this case, the resonance frequencies are

$$\omega_{in} = \sqrt{\frac{k' + k_{in}}{M}},\ \omega_{an} = \sqrt{\frac{k' + k_{an} + 2k_c}{M}} \tag{2}$$

In a clamped-clamped beam, the equivalent stiffness of the beam at its fundamental modes of vibration are:

$$k_n = C_n^2 \times \frac{EI}{L^4}, \tag{3}$$

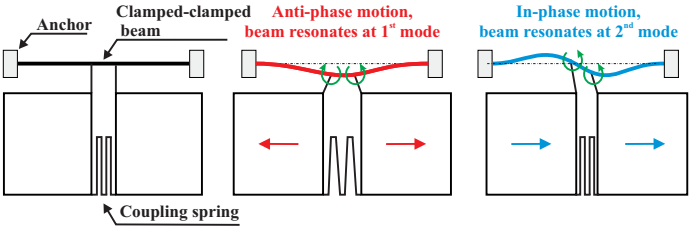

Fig. 3. The anti-phase and in-phase motion of proof masses excite the first and second flexural bending modes of the internal beam element, respectively.

where n is the mode number, E is Young's modulus of the material, I is the 2nd moment of area, L is the beam length, and C_n is the mode shape parameter of the beam. For a clamped-clamped beam, $C_1 = 22.37$ and $C_2 = 61.67$ impose a different stiffness on the in-phase and anti-phase motion ($k_{in} > k_{an}$). According to Eq. 2, the condition for mode ordering, $\omega_{an} < \omega_{in}$, is

$$k_c < \frac{k_{in} - k_{an}}{2}. \tag{4}$$

A weak coupling stiffness was configured to provide a large frequency separation between the anti-phase and the in-phase modes.

III. Device Characterization

The mode ordered DFP was designed with anti-phase resonance frequency of 20 kHz, as the first operational mode, separated by 12 kHz from the in-phase resonance mode, Fig. 4. The device was wire-bonded to a Leadless Chip Carrier (LCC) for characterization. A fully differential drive architecture (push-pull) was applied on the parallel-plate drive electrodes. Electromechanical Amplitude Modulation (EAM) at 300 kHz was implemented to eliminate the feed-through parasitics on the sense electrodes. The AC drive signal of 12 mV and the DC bias voltage of 1 V were used for the initial frequency response characterization. The mode-ordering was experimentally verified from the frequency sweep response, Fig. 5. A single-ended output channel was used to detect the in-phase resonance peak. The fabricated device revealed an anti-phase resonance frequency of 15 kHz, which is 5 kHz lower than the designed frequency.

A ringdown time measurement revealed a time constant of 3.7 seconds, corresponding to a quality factor higher than 170,000 on both modes. The encapsulated MEMS gyroscope

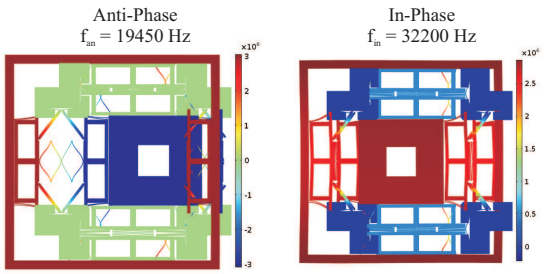

Fig. 4. Finite element simulation results of anti-phase and in-phase resonance modes of a mode ordered DFP with a clamped-clamped beam element.

was vented by defining a 8 μm vent hole through the cap wafer using Focused Ion Beam (FIB) milling. The characterization of the vented device in a vacuum chamber showed the ringdown time of 17.52 (s) and 17.24 (s) along the X- and Y- axes, corresponding to the quality factors higher than 820,000 at 20 $\mu Torr$, approaching the Q_{TED} of 1.1 million derived from finite element simulations. The vented device was vacuum sealed with an activated getter for a better vacuum stability and rate-table characterization. A thin layer of Cr/Au (500Å/3000Å) was deposited on the backside of the dies and Gold-Tin (Au80/Sn20) alloy was used for the eutectic die-attachment in the vacuum. The device was re-wire-bonded and vacuum sealed with getter in an ultra-high vacuum sealing process [11]. Fig. 6 illustrates the ringdown time of the vacuum sealed gyro, demonstrating quality factors higher than 700,000 in both modes. The lower quality factor after vacuum sealing was due to the disengagement of the cryogenic pump form the vacuum sealing furnace. The quality factor measurement results are summarized in Table I.

For the rate operation, the as-fabricated frequency mismatch of 112 Hz was electrostatically tuned to less than 100 mHz with 6.95 V DC tuning voltage. The Phase-Locked Loop (PLL) and Automatic Gain Control (AGC) Loop were implemented using Zurich Instruments HF2LI Lock-in Amplifier to drive the gyroscope into resonance. The open-loop scale factor of 1.26 mV/deg/sec was extracted by applying an incremental step input rotation from 10 to 90 deg/sec. Fig. 7 shows the Allan Deviation (ADEV) of the zero rate output (ZRO) bias of the mode-ordered DFP operating in the open-loop rate mode, revealing ARW of 0.075 $\mathrm{deg}/\sqrt{hr}$ and in-run bias stability of 1.9 deg/hr.

IV. Conclusion

A mode-ordered dual Foucault pendulum gyroscope at a center frequency of $\sim$ 15 kHz was designed and fabricated using epitaxial silicon encapsulation process. Quality factors higher than 700,000 were demonstrated after venting and vacuum sealing with getter activation. The high quality factor is associated with a dynamically balanced operation of the device in the anti-phase motion. The implemented new suspension and coupling design provided $\sim$ 12kHz frequency separation between the desired and spurious frequency modes, ordered the anti-phase mode as the first vibration mode of the device. The initial open-loop rate gyro characterization results revealed ARW of 0.075 $\mathrm{deg}/\sqrt{hr}$ and in-run bias stability of 1.9 deg/hr, without temperature control in the lab environment. The high quality factor and mode-ordered DFP operating in the degenerate mode can be possibly utilized for a reliable rate measurement in harsh environments.

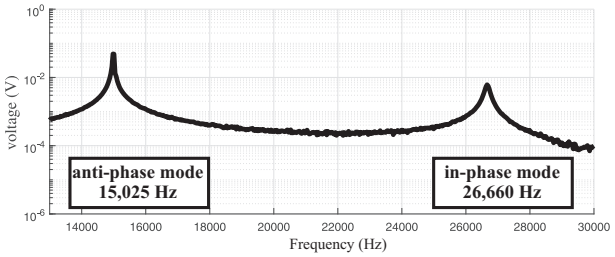

Fig. 5. Frequency sweep response shows the mode-ordered anti-phase and in-phase resonances with $\sim$ 11.5 kHz frequency separation.

TABLE I
Quality Factor of Mode Ordered DFP Gyroscope

	Episeal (as-fabricated)	Vented in vacuum chamber at 20 μTorr	Vacuum sealed with getter
X-axis	τ = 2.7 s Q = 127,000	τ = 17.22 s Q = 812,000	τ = 15.13 s Q = 714,000
Y-axis	τ = 2.8 s Q = 133,000	τ = 17.52 s Q = 833,000	τ = 15.21 s Q = 723,000

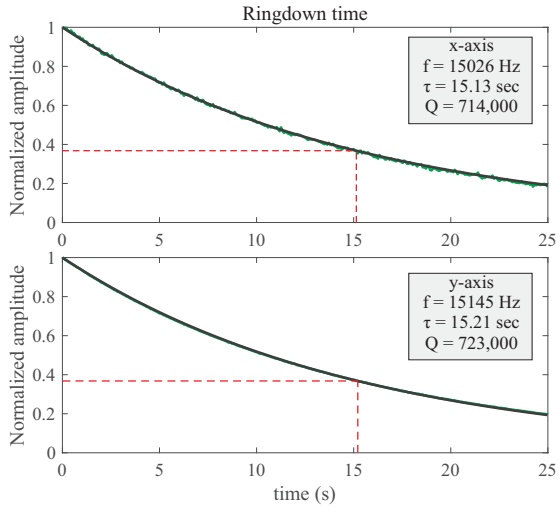

Fig. 6. Quality factors higher than 700,000 on both modes of the mode-ordered DFP after vacuum sealing with getter.

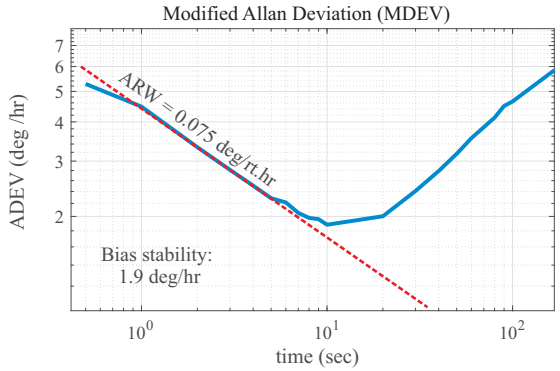

Fig. 7. ADEV plot of the gyroscope open-loop rate output showing ARW of 0.075 $\mathrm{deg}/\sqrt{hr}$ and bias stability of 1.9 deg/hr.

Acknowledgment

This work was supported by the Defense Advanced Research Projects Agency (DARPA) and U.S. Navy under Contract No. N66001-16-1-4021 at UC Irvine and Contract No. N66001-16-1-4023 at Stanford University. The fabrication work was performed in part at the Stanford Nanofabrication Facility (SNF), supported by the National Science Foundation under Grand ECS- 9731293.

REFERENCES

[1] V. Kaajakari *et al.*, "Practical mems: Design of microsystems, accelerometers, gyroscopes, rf mems, optical mems, and microfluidic systems," *Las Vegas, NV: Small Gear Publishing*, 2009.

[2] M. F. Zaman, A. Sharma, and F. Ayazi, "High performance matched-mode tuning fork gyroscope," in *the IEEE Micro Electro Mechanical Systems (MEMS), Istanbul, Turkey*, Jan. 2006.

[3] D. Vatanparvar and A. M. Shkel, "Effect of fabrication imperfections on energy loss through mechanical mode coupling in mems," in *2018 IEEE International Symposium on Inertial Sensors and Systems (INERTIAL), Lake Como, Italy*, March 2018.

[4] J. Bernstein, S. Cho, A. T. King, A. Kourepenis, P. Maciel, and M. Weinberg, "A micromachined comb-drive tuning fork rate gyroscope," in *the IEEE Micro Electro Mechanical Systems (MEMS),Fort Lauderdale, FL, USA*, Feb. 1993.

[5] D. Senkal, A. Efimovskaya, and A. M. Shkel, "Dual foucault pendulum gyroscope," in *the International Conference on Solid-State Sensors, Actuators and Microsystems (TRANSDUCERS), Anchorage, Alaska, USA*, June 2015.

[6] J. Giner, Y. Zhang, D. Maeda, K. Ono, A. M. Shkel, and T. Sekiguchi, "Dynamicaly balanced degenerate mode gyro with sub-hz frequency symmetry and temperature robustness," in *the IEEE Micro Electro Mechanical Systems (MEMS), Las Vegas, NV, USA*, Jan. 2017.

[7] M. F. Zaman, A. Sharma, Z. Hao, and F. Ayazi, "A mode-matched silicon-yaw tuning-fork gyroscope with subdegree-per-hour allan deviation bias instability," *Journal of Microelectromechanical Systems*, vol. 17, no. 6, pp. 1526–1536, Dec. 2008.

[8] S. Askari, M. H. Asadian, K. Kakavand, and A. M. Shkel, "Near-Navigation Grade Quad Mass Gyroscope with Q-factor Limited by Thermo-Elastic Damping," in *the Solid-State Sensors, Actuators, and Microsystems Workshop, Hilton Head Island, SC, USA*, June 2016.

[9] I. B. Flader, Y. Chen, C. H. Ahn, D. D. Shin, A. L. Alter, J. Rodriguez, and T. W. Kenny, "Epitaxial encapsulation of fully differential electrodes and large transduction gaps for mems resonant structures," in *the IEEE Micro Electro Mechanical Systems (MEMS), Belfast, Northern Ireland*, Jan. 2018.

[10] B. R. Simon, S. Khan, A. A. Trusov, and A. M. Shkel, "Mode ordering in tuning fork structures with negative structural coupling for mitigation of common-mode g-sensitivity," in *the IEEE Sensors, Busan, South Korea*, Nov. 2015.

[11] M. H. Asadian, S. Askari, and A. M. Shkel, "An ultrahigh vacuum packaging process demonstrating over 2 million q-factor in mems vibratory gyroscopes," *IEEE Sensors Letters*, vol. 1, no. 6, pp. 1–4, Dec. 2017.